Learning Wideband User Scheduling and Hybrid Precoding with Graph Neural Networks

Shengjie Liu, Chenyang Yang, and Shengqian Han

Abstract—Spatial-frequency scheduling and hybrid precoding in wideband multi-user multi-antenna systems have never been learned jointly due to the challenges arising from the massive user combinations on resource blocks (RBs) and the shared analog precoder among RBs. In this paper, we strive to jointly learn the scheduling and precoding policies with graph neural networks (GNNs), which have emerged as a powerful tool for optimizing resource allocation thanks to their potential in generalizing across problem scales. By reformulating the joint optimization problem into an equivalent functional optimization problem for the scheduling and precoding policies, we propose a GNN-based architecture consisting of two cascaded modules to learn the two policies. We discover a same-parameter same-decision (SPSD) property for wireless policies defined on sets, revealing that a GNN cannot well learn the optimal scheduling policy when users have similar channels. This motivates us to develop a sequence of GNNs to enhance the scheduling module. Furthermore, by analyzing the SPSD property, we find when linear aggregators in GNNs impede size generalization. Based on the observation, we devise a novel attention mechanism for information aggregation in the precoder module. Simulation results demonstrate that the proposed architecture achieves satisfactory spectral efficiency with short inference time and low training complexity, and is generalizable to the numbers of users, RBs, and antennas at the base station and users.

Index Terms—Hybrid precoding, user scheduling, wideband, graph neural network, attention mechanism.

I. INTRODUCTION

TBRID analog and baseband precoding stands as a pivotal technique for supporting high spectral efficiency (SE) in millimeter wave multiple-input multiple-output (MIMO) systems [2]. While the decreased number of radio frequency (RF) chains reduces the hardware and energy costs, it also imposes a constraint on the number of users served on each resource block (RB) in each time slot.

In wideband MIMO systems, hybrid precoding and spatial-frequency user scheduling are coupled, making their optimization highly challenging. Specifically, the analog precoder, shared among all RBs in orthogonal frequency division multiplexing (OFDM) systems [3], couples the scheduling decisions across RBs, thereby impeding the direct application of existing narrow-band user scheduling methods on each RB. The computational complexity of exhaustively searching all possible user combinations grows exponentially with the numbers of candidate users and RBs [4]. To avoid the prohibitive complexity of jointly optimizing spatial-frequency scheduling and hybrid precoding, several heuristic methods were proposed, say imposing zero-forcing (ZF) constraint on precoding in linear successive allocation (LISA) [5], combining greedy scheduling with ZF precoder [6], or ignoring the multi-user

The codes will be open-sourced if the manuscript is accepted. A part of this work has been presented in IEEE WCNC 2024 [1]. The authors are with Beihang University, Beijing 100191, China.

interference (MUI) during scheduling [7]. However, these methods still entail considerable computational costs or lead to evident performance degradation.

To facilitate real-time implementation, learning-based methods have been developed. Wireless policies, which map environment parameters such as channels into resource allocation outcomes, can be learned by deep neural networks (DNNs) with short inference time. Yet, to the best of our knowledge, the study of jointly learning spatial-frequency user scheduling and hybrid precoding has never been reported.

A. Related Works

1) Learning precoding and scheduling policies: Most previous works studied the learning of precoding and scheduling in narrow-band systems. A majority of these studies learned to optimize scheduling with a pre-determined precoder, where the DNNs were trained in a supervised manner [8, 9] or by reinforcement learning (RL) [10,11] to deal with the difficulty of learning "0-1" variables. In [8], a fully-connected neural network (FNN) was applied to learn a scheduling policy given maximum ratio transmission. In [9], Transformer [12] was used to select users with an existing approach for learning combinatorial problems, where ZF precoder was considered. In [10], an FNN was trained by RL to optimize scheduling, given a baseband precoder that maximizes signal-to-leakageand-noise ratio. In [11], RL was also adopted for user scheduling, given an analog precoder comprising the eigenvectors of channel covariance matrix and a ZF baseband precoder.

Several recent works attempted to learn both scheduling and precoding policies in narrow-band systems. In [13], an FNN integrated with attention mechanism was applied to schedule users and choose analog precoder from a codebook, where the baseband precoding was solved with an existing numerical algorithm. In [14], two graph neural networks (GNNs), respectively designed for user scheduling and reconfigurable intelligent surface (RIS) configuration, were trained separately with unsupervised learning, and then the weighted minimum mean square error (WMMSE) algorithm was used for optimizing precoding. In [15], a RIS configuration and baseband precoder module was trained by an RL algorithm, then the module was fixed for training a scheduler module with another RL algorithm, and the two modules were not trained jointly. To jointly optimize user scheduling and baseband precoding in narrow-band multi-user multiple-input single-output (MU-MISO) systems, a GNN was designed in [16], where the structure of the optimal precoder matrix was harnessed to simplify the functions to be learned. However, the method is problem-specific and not applicable to wideband or hybrid precoding systems.

For wideband systems, the learning of scheduling was studied in [4], where two FNNs were employed as actor and critic networks. Although analog precoder was not involved, the scheduling problem is coupled across RBs due to the objective of user fairness. However, a ZF precoder was used and the joint learning was not investigated in [4].

2) Learning to optimize with GNNs: GNNs have been shown to surpass FNNs and convolutional neural networks (CNNs) in terms of training efficiency and the potential in size generalizability [17]. GNNs, exploiting the permutation prior of wireless policies, such as permutation equivariance (PE) and permutation invariance (PI), learn policies in smaller hypothesis spaces, thereby reducing training complexity. Once trained, GNNs can be applied across varying system scales. However, their generalization performance is not guaranteed especially when learning precoding policies. It can be observed from simulation results in the literature that the generalizability differs among different types of sizes. For example, GNNs need to be judiciously designed to be generalized well to the number of users [18], whereas GNNs using linear aggregator can achieve favorable generalization performance to the number of antennas [19, 20].

3) Attention mechanism for precoding: In order to improve the learning performance and size generalizability, attention mechanism has been introduced for optimizing precoding. In [15, 21], the attention mechanism in Transformer [12] was employed to capture MUI and boost SE. In [22, 23], graph attention network (GAT) [24] was used to learn over a graph with only user vertices to enable generalizability to the number of users. In [25], Transformer was regarded as a GNN, which was shown generalizable to the number of users. In [18, 19], attention mechanisms were designed for the edge-GNNs, where edge representations were updated to facilitate generalizability to the number of users. Notwithstanding, all aforementioned works consider narrow-band MU-MISO systems. The designed attention mechanisms are not applicable to wideband MU-MIMO systems.

B. Motivation and Contributions

Although existing works studied the learning of scheduling and precoding, the joint learning of spatial-frequency scheduling, hybrid precoding, and analog combining remains unsolved. This problem involves learning multiple high-dimensional decisions, necessitating efficient DNN designs.

Previous studies have recognized that GNN is a powerful tool for optimizing precoding, with the potential in generalizing across problem scales, particularly when associated with attention mechanisms. However, incorporating an attention mechanism is not always beneficial in generalizability while adding computation complexity. Unfortunately, existing studies lack the foresight to identify which types of sizes GNNs struggle to generalize well without attention mechanisms. As a result, extensive trial-and-error procedures are required for the design of GNNs. Therefore, it is crucial to determine which types of information should be aggregated using attention mechanisms when designing GNNs.

In this paper, we propose a GNN-based architecture to jointly learn spatial-frequency scheduling, hybrid precoding,

and analog combining in downlink wideband MU-MIMO systems. Simulation results are provided to evaluate the proposed architecture in terms of learning performance, size generalizability, training complexity, and inference time by comparing it with numerical algorithms and other DNNs.

The major contributions are summarized as follows.

- We transform the joint optimization problem into a functional optimization problem for a two-layer nested policy, consisting of an inner scheduling policy (corresponding to spatial-frequency scheduling) and an outer precoding policy (corresponding to hybrid precoding and analog combining). To learn the two policies, we propose an architecture comprising a scheduler module and a precoder module, which can be jointly trained in an unsupervised manner to enhance learning performance. Both modules are designed as GNNs that satisfy the complex permutation properties of the two policies, thereby reducing training complexity and achieving size generalizability.
- To provide guidance for designing GNNs with good size generalizability and learning performance, we discover a same-parameter same-decision (SPSD) property for the optimization problems and resulting policies defined on sets. This property impacts GNNs in two ways. First, we observe that GNNs with linear aggregators can be generalized to the size of a set when the policy to be learned is SPSD on the set, making attention mechanism unnecessary. Second, we find a mismatch between the functions learned by GNNs and non-SPSD policies, resulting in a challenge for GNNs in learning these policies when some environment parameters are similar.
- We find that the precoding policy is non-SPSD on the user set, leading to poor generalizability to the number of users with linear aggregators. To address this, we devise a partial attention mechanism for the GNN in the precoder module, which can distinguish the importance of different users with multiple antennas on every RB during information aggregation.
- We find that the scheduling policy is non-SPSD on the user set, causing a single GNN unable to well learn the scheduling policy when users have similar channels. To tackle this, we propose a sequence of GNNs as an enhancement of the scheduling module to improve the learning performance in high-density user scenarios.

Compared to the conference version [1], this journal version finds the SPSD property, extends the problem from narrow-band scheduling and hybrid precoding to wideband spatial-frequency scheduling, hybrid precoding and combining, develops a novel GNN architecture with reduced training and inference complexities, and provides more simulation results for both performance and complexity comparisons.

The rest of the paper is organized as follows. Sec. II introduces the SPSD property and its impacts on GNNs. Sec. III introduces the joint scheduling and precoding problem and the two policies to be learned. Sec. IV proposes our architecture and analyzes its computational complexity. Sec. V provides simulation results. Sec. VI provides conclusions.

Notations: ① denotes the element-wise product of two vectors. \otimes denotes the Kronecker product of two matrices.

3

 Π denotes permutation matrix. $\pi(\cdot)$ maps the *i*th element in a set into the $\pi(i)$ th element. $(\mathbf{X})_{i_1,\dots,i_N}$ denotes an element with index i_1,\dots,i_N in an N-dimensional array \mathbf{X} .

II. SPSD PROPERTY OF WIRELESS POLICIES

In this section, we introduce the SPSD property of wireless policies defined on sets and discuss the impacts of the property.

A. SPSD Property

A wireless policy is a mapping from the environment parameters to the optimal solutions of an optimization problem. Wireless policies obtained from the problems consisting of sets are with permutation properties [19]. For instance, consider the following optimization problem

$$P_1: \max_{\mathbf{w}_1, \dots, \mathbf{w}_N} F_0(\mathbf{w}_1, \dots, \mathbf{w}_N, \mathbf{h}_1, \dots, \mathbf{h}_N),$$

s.t. $F_i(\mathbf{w}_1, \dots, \mathbf{w}_N, \mathbf{h}_1, \dots, \mathbf{h}_N) \leq 0, i = 1, \dots, N_C,$

where $F_0(\cdot)$ is the objective function, $F_i(\cdot)$ is the *i*th constraint function, and N is the problem scale.

The policy obtained from P_1 is the mapping from the environment parameters $\mathbf{h}_1, \dots, \mathbf{h}_N$ to the corresponding optimal decisions $\mathbf{w}_1, \dots, \mathbf{w}_N$, denoted as $(\mathbf{w}_1, \dots, \mathbf{w}_N) = f(\mathbf{h}_1, \dots, \mathbf{h}_N)$. The policy $f(\cdot)$ is a multivariate function if P_1 has a unique optimal solution. It is not a function if multiple optimal solutions exist, since a function is a one-to-one or many-to-one mapping.

 P_1 involves a set of size N, which is $\{1,\ldots,N\} \triangleq \mathcal{N}$. If permuting the indices $\{1,\cdots,N\}$ into $[\pi(1),\cdots,\pi(N)]^T = \mathbf{\Pi}^T[1,\cdots,N]^T$ does not change the objective and constraint functions of P_1 , then the policy $f(\cdot)$ satisfies the *PE property*, i.e., $(\mathbf{w}_{\pi(1)},\cdots,\mathbf{w}_{\pi(N)}) = f(\mathbf{h}_{\pi(1)},\cdots,\mathbf{h}_{\pi(N)})$ [19], and $f(\cdot)$ is called a PE-policy.

The decisions $\mathbf{w}_1, \dots, \mathbf{w}_N$ are the optimal solution corresponding to a group of parameters $\mathbf{h}_1, \dots, \mathbf{h}_N$. If $\mathbf{h}_i = \mathbf{h}_j$, then $\mathbf{w}_i = \mathbf{w}_j$ or $\mathbf{w}_i \neq \mathbf{w}_j$ depending on the problem.

Definition 1: (*PE-*)*SPSD property.* Assume that $\mathbf{h}_i = \mathbf{h}_j, i \neq j$. If the optimal solution of P_1 yields $\mathbf{w}_i = \mathbf{w}_j$, then problem P_1 and the PE-policy $f(\cdot)$ are PE-SPSD or simply SPSD on the set \mathcal{N} . If $\mathbf{w}_i \neq \mathbf{w}_j$, then P_1 and $f(\cdot)$ are non-SPSD on the set \mathcal{N} .

To help understand the property, we provide two examples. **Example 1:** Narrow-band MU-MISO precoding. The precoding problem for SE maximization under the transmit power constraint consists of two sets. One set is composed of K users, and the other set is composed of N_T antennas. The corresponding precoding policy can be expressed as $(\mathbf{w}_1, \cdots, \mathbf{w}_K) = f(\mathbf{h}_1, \cdots, \mathbf{h}_K)$, which is defined on user set with $\mathbf{w}_k, \mathbf{h}_k \in \mathbb{C}^{N_T \times 1}$. The policy can also be expressed as $(\tilde{\mathbf{w}}_1, \cdots, \tilde{\mathbf{w}}_{N_T}) = f(\tilde{\mathbf{h}}_1, \cdots, \tilde{\mathbf{h}}_{N_T})$, which is defined on antenna set with $\tilde{\mathbf{w}}_n, \tilde{\mathbf{h}}_n \in \mathbb{C}^{K \times 1}$. It is not hard to prove that this problem and the policy are SPSD on antenna set, but are non-SPSD on user set.

Example 2: Power control in interference channels. The power control problem for SE maximization in an interference system with two transceiver pairs consists of one set, i.e., the set of transceiver pairs. As proved in Appendix A, the SPSD property of this problem and the policy depends on the value of a threshold s_h related to channel gains. They are SPSD for large s_h but non-SPSD for small s_h .

Definition 2: *PI-SPSD property.* Consider the policy $\mathbf{w} = \overline{f(\mathbf{h}_1, \dots, \mathbf{h}_N)}$. If the policy exhibits the *PI property* on \mathcal{N} , i.e., $\mathbf{w} = f(\mathbf{h}_{\pi(1)}, \dots, \mathbf{h}_{\pi(N)})$, then the policy is PI-SPSD.

The PI-SPSD property can be regarded as a special case of PE-SPSD. To see this, one can rewrite the PI-policy $\mathbf{w} = f(\mathbf{h}_1, \dots, \mathbf{h}_N)$ as $(\mathbf{w}_1, \dots, \mathbf{w}_N) = f(\mathbf{h}_1, \dots, \mathbf{h}_N)$ subject to $\mathbf{w}_1 = \dots = \mathbf{w}_N = \mathbf{w}$, which is naturally SPSD.

B. Impacts of SPSD Property on GNNs

1) <u>Impact on Size Generalization</u>: A GNN can satisfy the permutation property of a policy via a proper design. After training, the GNN can be used for different problem scales. However, the generalization performance is not guaranteed.

From empirical evaluations in the literature, we can observe that the size generalizability of GNNs is affected by the SPSD property of a policy. Taking the MU-MISO precoding policy (i.e., Example 1) as an instance, a GNN satisfying the PE properties on both user and antenna sets is easy to be generalized to the number of antennas [19, 20]. That is, the GNN achieves satisfactory generalization performance to the number of antennas, even if the information from different antennas are simply linearly aggregated in the update process. However, the GNN can be generalized to the number of users only if its update equation is judiciously designed [18], since the policy is non-SPSD on user set.

2) Impact on Learning Performance: function The learned by a GNN over a graph with N vertices can be denoted as $(\mathbf{w}_1, \dots, \mathbf{w}_i, \dots, \mathbf{w}_i, \dots, \mathbf{w}_N)$ $g(\mathbf{h}_1, \dots, \mathbf{h}_i, \dots, \mathbf{h}_j, \dots, \mathbf{h}_N)$. When the GNN satisfies the same PE property as the policy to be learned, \mathbf{w}_i and \mathbf{w}_i will be swapped if h_i and h_i are swapped. Thus, the function can also be expressed as $(\mathbf{w}_1, \dots, \mathbf{w}_j, \dots, \mathbf{w}_i, \dots, \mathbf{w}_N) =$ $g(\mathbf{h}_1, \dots, \mathbf{h}_j, \dots, \mathbf{h}_i, \dots, \mathbf{h}_N)$. If $\mathbf{h}_i = \mathbf{h}_j$, the two groups of inputs become identical, and the corresponding two groups of outputs will also be identical, which implies $\mathbf{w}_i = \mathbf{w}_j$, since a GNN learns functions rather than mappings. This indicates that a GNN cannot learn the optimal solution of a non-SPSD problem when some of the environment parameters are identical. Even though it is unlikely for two environment parameters to be exactly same in practice, learning a non-SPSD policy with a GNN is challenging for achieving good performance. This is because a GNN produces continuous functions, leading to $\mathbf{w}_i \approx \mathbf{w}_j$ if $\mathbf{h}_i \approx \mathbf{h}_j$.

III. SCHEDULING AND PRECODING POLICIES

In this section, we formulate the joint scheduling and precoding problem in wideband MU-MIMO systems, and transform it into a functional optimization without loss of optimality. Then, we analyze the permutation properties and SPSD properties of the scheduling and precoding policies.

A. Joint Scheduling and Precoding Optimization Problem

Consider a downlink MU-MIMO OFDM system, where a BS equipped with N_T antennas and $N_{\rm RF}$ RF chains serves K candidate users over M RBs. Each RF chain is connected to all antennas [3]. Each user has N_R antennas and one RF chain. At most K' users can be scheduled on each RB, where $K' \leq N_{\rm RF}$. A hybrid analog and baseband precoding is used for K' scheduled users.

We first introduce some notations.

- Channels: $\mathbf{H} \in \mathbb{C}^{M \times KN_R \times N_T}$ represents the wideband channels from the BS to all candidate users. $\mathbf{H}_m \in \mathbb{C}^{KN_R \times N_T}$ is the channel matrix of all candidate users on the mth RB. $\mathbf{H}_{m,k} \in \mathbb{C}^{N_R \times N_T}$ is the channel matrix of the kth user on the mth RB. $\mathbf{h}_{m,kr} \in \mathbb{C}^{N_T \times 1}$ is the channel vector to the rth receive antenna at the kth user on the mth RB.
- Analog precoder: $\mathbf{W}_{RF} \in \mathbb{C}^{N_T \times N_{RF}}$ denotes the analog precoding matrix.
- Baseband precoder: $\mathbf{W}_{\mathrm{BB}} \in \mathbb{C}^{M \times N_{\mathrm{RF}} \times K}$ represents the wideband baseband precoders of all candidate users. $\mathbf{W}_{\mathrm{BB}m} \in \mathbb{C}^{N_{\mathrm{RF}} \times K}$ is the baseband precoding matrix of all candidate users on the mth RB. $\mathbf{w}_{\mathrm{BB}m,k} \in \mathbb{C}^{N_{\mathrm{RF}} \times 1}$ is the baseband precoding vector of the kth user on the mth RB.
- Analog combiner: $\mathbf{v}_{\mathrm{RF}} \in \mathbb{C}^{KN_R \times 1}$ denotes the analog combining vector of all candidate users. $\mathbf{v}_{\mathrm{RF}k} \in \mathbb{C}^{N_R \times 1}$ denotes the analog combining vector of the kth user.
- Scheduler decision: $\mathbf{A} \in \{0,1\}^{M \times K}$ denotes the scheduling matrix. $\mathbf{a}_m \in \{0,1\}^{1 \times K}$ denotes the scheduling decisions on the mth RB. $a_{m,k} \in \{0,1\}$ indicates whether the kth user is scheduled on the mth RB.
- Notations for scheduled users: we use H', W'_{BB}, and v'_{RF} to denote the counterparts of the notations for K' scheduled users, which have the same dimensions as H, W_{BB}, and v_{RF}, but with K' replacing K.

Spatial-frequency scheduling, hybrid precoding, and analog combing can be optimized jointly, say to maximize SE as follows [5,26],

$$P_{\mathbf{A}, \mathbf{v}_{\mathsf{RF}}, \mathbf{W}_{\mathsf{RF}}, \mathbf{W}_{\mathsf{BB}}} R(\mathbf{A}, \mathbf{v}_{\mathsf{RF}}, \mathbf{W}_{\mathsf{RF}}, \mathbf{W}_{\mathsf{BB}}; \mathbf{H}) \triangleq \frac{1}{M} \sum_{m=1}^{M} \sum_{k=1}^{K} R_{m,k}$$

s.t.
$$\sum_{m=1}^{M} \sum_{k=1}^{K} a_{m,k} \|\mathbf{W}_{RF} \mathbf{w}_{BBm,k}\|_{2}^{2} = P_{tot},$$
 (1a)

$$|(\mathbf{W}_{RF})_{n,j}| = 1, n = 1, \dots, N_T, j = 1, \dots, N_{RF},$$
 (1b)

$$|(\mathbf{v}_{RF})_{kr}| = 1, k = 1, \cdots, K, r = 1, \cdots, N_R,$$
 (1c)

$$a_{m,k} \in \{0,1\}, m = 1, \cdots, M, k = 1, \cdots, K,$$
 (1d)

$$\sum_{k=1}^{K} a_{m,k} \le K', m = 1, \cdots, M, \tag{1e}$$

where $R_{m,k}$ is the data rate of the kth user on the mth RB, $R_{m,k} = \log_2 \left(1 + \frac{a_{m,k} |\mathbf{v}_{\mathsf{RFk}}^H \mathbf{H}_{m,k} \mathbf{W}_{\mathsf{RF}} \mathbf{w}_{\mathsf{BB}m,k}|^2}{\sum_{\substack{i=1 \ i \neq k}}^K a_{m,i} |\mathbf{v}_{\mathsf{RFk}}^H \mathbf{H}_{m,k} \mathbf{W}_{\mathsf{RF}} \mathbf{w}_{\mathsf{BB}m,i}|^2 + N_R \sigma^2}\right), \text{ and}$

 σ^2 is noise power that is amplified by $\mathbf{v}_{RFk}^H \mathbf{v}_{RFk} = N_R$.

In problem P_J , constraint (1a) is the total power constraint, (1b) and (1c) are respectively the constant modulus constraints for analog precoder and analog combiners, and (1e) restricts the maximal number of scheduled users on each RB. In fact, tightening constraint (1e) as

$$\sum_{k=1}^{K} a_{m,k} = K', m = 1, \cdots, M$$
 (2)

does not affect the optimality. This is because both $a_{m,k} = 0$ and $\mathbf{w}_{\mathrm{BB}m,k} = \mathbf{0}$ indicate not to schedule the kth user on the mth RB. In other words, the optimal baseband precoder will allocate zero power to the unscheduled users, even if their indicators are "1"s.

B. Problem Reformulation and Two Policies to be Learned

According to the proof in [27], the parameter optimization problem P_J can be equivalently transformed into a functional optimization problem with respect to the joint policy $(\mathbf{A}, \mathbf{v}_{RF}, \mathbf{W}_{RF}, \mathbf{W}_{BB}) = f_J(\mathbf{H})$, which can be formulated as

$$P_F : \max_{f_J(\cdot)} \mathbb{E} \left\{ R(f_J(\mathbf{H}); \mathbf{H}) \right\}$$

s.t. $(1a) \sim (1d), (2),$

where $f_J(\cdot)$ maps channels **H** to the optimal solution of problem P_J , and the expectation $\mathbb{E}\{\cdot\}$ is taken over the random channels **H**.

Learning-based methods employ DNNs to parameterize the policy $f_J(\cdot)$. However, directly learning the joint policy $f_J(\cdot)$ as in [1] entails an excessive number of invalid decisions, such as the precoding and combining vectors for unscheduled users. This significantly increases learning complexity.

To avoid learning invalid decisions, we transform the joint policy into a two-layer nested policy. Specifically, the inner layer is the *scheduling policy*, denoted by $\mathbf{A} = f_S(\mathbf{H})$, while the outer layer is the *precoding policy* learning precoders and combiners only for the scheduled users, denoted by $(\mathbf{v}'_{RF}, \mathbf{W}_{RF}, \mathbf{W}'_{BB}) = f_P(\mathbf{H}')$. The channels of scheduled users \mathbf{H}' is selected from \mathbf{H} based on the value of \mathbf{A} and can be obtained as

$$\mathbf{H}' = f_H(\mathbf{H}, \mathbf{A}) \in \mathbb{C}^{M \times K' N_R \times N_T}, \tag{4}$$

where the function $f_H(\cdot)$ will be detailed in the next section. Upon substituting $f_S(\cdot)$ into (4) and then into $f_P(\cdot)$, we can obtain the two-layer nested policy as

$$(\mathbf{v}_{RF}', \mathbf{W}_{RF}, \mathbf{W}_{BB}') = f_P(f_H(\mathbf{H}, f_S(\mathbf{H}))). \tag{5}$$

Considering that the unscheduled users contribute zero data rate, the objective of problem P_J is equal to

$$R'\left(\mathbf{v}_{RF}', \mathbf{W}_{RF}, \mathbf{W}_{BB}'; \mathbf{H}'\right) \triangleq \frac{1}{M} \sum_{m=1}^{M} \sum_{k'=1}^{K'} R'_{m,k'}, \qquad (6)$$

where
$$R'_{m,k'} = \log_2 \left(1 + \frac{|\mathbf{v}_{\text{RF}k'}^{'H} \mathbf{H}'_{m,k'} \mathbf{W}_{\text{RF}} \mathbf{w}_{\text{BB}m,k'}^{'}|^2}{\sum_{\substack{i=1 \ i \neq k'}}^{K'} |\mathbf{v}_{\text{RF}k'}^{'H} \mathbf{H}'_{m,k'} \mathbf{W}_{\text{RF}} \mathbf{w}_{\text{BB}m,i}^{'}|^2 + N_R \sigma^2} \right).$$

Consequently, P_F can be equivalently transformed into the following functional optimization problem with respect to $f_P(f_H(\mathbf{H}, f_S(\mathbf{H})))$:

$$P_N: \max_{f_P(f_H(\cdot,f_S(\cdot)))} \mathbb{E}\left\{R'\left(f_P(f_H(\mathbf{H},f_S(\mathbf{H}))); f_H(\mathbf{H},f_S(\mathbf{H}))\right)\right\}$$

s.t.
$$\sum_{m=1}^{M} \sum_{k'=1}^{K'} \|\mathbf{W}_{RF}\mathbf{w}'_{BBm,k'}\|_{2}^{2} = P_{tot},$$
 (7a)

$$|(\mathbf{v}'_{RF})_{k'r}| = 1, k' = 1, \dots, K', r = 1, \dots, N_R,$$
 (7b) (1b), (1d), (2).

Problem P_N is equivalent to P_F in the sense that they have the same optimal objective.

From (5), we can observe that the input to the outer policy $f_P(\cdot)$ depends on the inner policy $f_S(\cdot)$, indicating that $f_P(\cdot)$ has to be jointly optimized with $f_S(\cdot)$. To achieve this, we propose a cascaded architecture to jointly learn the two policies, where a *scheduler module* learns $f_S(\cdot)$ and a *precoder module* learns $f_P(\cdot)$. The output of the scheduler module is passed to $f_H(\cdot)$, and the resulting output is then passed to the

precoder module. Both modules are parameterized as DNNs and require joint training to optimize their performance.

C. Permutation Properties of the Two Policies

To enhance training efficiency and ensure size generalizability, we employ GNN to realize the two modules in the proposed architecture. To construct the graphs for the GNNs, we analyze the permutation properties of the two policies.

According to the method given in [19], the permutation properties can be analyzed by identifying sets relevant to a policy. We can find three sets related to the two policies: RB, BS antenna (ANBS), and user antenna (ANUE). The RB set comprises M RBs. The ANBS set comprises N_T antennas at the BS. The ANUE set is a nested set, consisting of subsets (each for a user). Specifically, for scheduling, the ANUE set comprises K subsets, each containing N_R antennas. For precoding, the ANUE set comprises K' subsets, each containing N_R antennas. For brevity, we refer to the whole ANUE set as a user set with K (or K') "elements", each "element" is a subset, denoted as an N set.

In Table I, we summarize the permutation properties of the two policies with respect to each of these sets, instead of expressing the properties using the permutation matrices as in [19]. To aid in understanding the table, we elaborate on the first two rows in the "RB" column: a) For the scheduling policy, if the indices of RBs are permuted in \mathbf{H} , the indices of RBs in scheduling decision \mathbf{A} will be permuted equivariantly. b) If the indices of RBs are permuted in \mathbf{H}' , the precoding decision \mathbf{v}'_{RF} will remain unchanged (i.e., invariant), since the analog combiner is shared among all RBs.

TABLE I
PERMUTATION AND SPSD PROPERTIES OF THE TWO POLICIES

| | Set | RB | ANBS | AN ^{UE} (nested) | | |
|------------|-----------------------------|---------|---------|---------------------------|---------|--|
| Policy | | KD | AIN | User | AN | |
| Scheduling | Α | PE SPSD | PI SPSD | PE SPSD/non-SPSD | PI SPSD | |
| Precoding | \mathbf{v}_{RF}' | | PI SPSD | | PE SPSD | |
| | | | | | PI SPSD | |
| | $\mathbf{W}_{\mathrm{BB}}'$ | PE SPSD | PI SPSD | PE non-SPSD | PI SPSD | |

D. SPSD Properties of the Two Policies

SPSD properties can be identified from numerical algorithms with manually generated channels. For example, by duplicating one channel matrix on two RBs in a three-dimensional channel array and inputting the array into a numerical algorithm such as LISA [5], we can find that the scheduling and precoding policies are SPSD on RB set because the same decisions can be observed on both RBs.

The SPSD properties of the two policies are also presented in Table I. The scheduling policy on user set may exhibit SPSD or non-SPSD property, depending on the channels. For instance, for the two users having the same channel, if the channel is weak, then neither will be scheduled, resulting in an SPSD property. Conversely, if the channel is strong, only one user will be scheduled, leading to a non-SPSD property.

As discussed in Sec. II-B, the impact of the SPSD property is two-fold. Regarding generalization performance, the GNNs in both modules can be easily generalized to the size of RBs (M), antennas at the BS (N_T) , and antennas at each user (N_R) , because both policies are SPSD on these sets. The GNN in the

scheduler module can also be easily generalized to the number of users (K), since the scheduling policy tends to be SPSD on user set for most samples. By contrast, the GNN in the precoder module requires careful design to be generalized to K (when K < K'). If $K \ge K'$, the precoder module always serves K' users on each RB and does not need to generalize beyond this number.

Regarding learning performance, the GNN in the scheduler module faces challenges when learning the scheduling policy in scenario with densely distributed users. In such scenario, two users are likely to have similar channels, and the GNN schedules both or neither of them, leading to a mismatch with the non-SPSD scheduling policy and degradation in scheduling performance. On the other hand, although the precoding policy is always non-SPSD on the user set, the performance of the GNN in the precoder module does not degrade because no users have similar channels after the scheduling.

IV. GNN-BASED ARCHITECTURE FOR JOINT LEARNING

In this section, we propose the GNN-based architecture including the scheduler and precoder modules. To facilitate joint training of the two modules, we design a differentiable $f_H(\cdot)$ that connects the two modules. Then, we construct graphs and design GNNs for the two modules. To improve the scheduling performance in crowded user scenarios, we proceed to design a sequence of GNNs for the scheduler module. To allow size generalizability, we design a partial attention mechanism for the precoder module. Finally, we introduce the training and testing procedures and analyze the inference complexity.

The scheduler module can be realized as either a single GNN or a sequence of GNNs as an enhancement. This leads to two variants of the whole architecture, which are respectively referred to as non-sequential GNN (NGNN) and sequential GNN (SGNN). The NGNN architecture is shown in Fig. 1

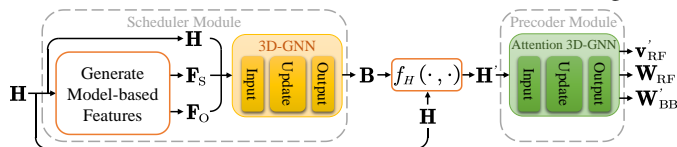


Fig. 1. NGNN architecture. The GNN in scheduler module is a 3D-GNN, and the GNN in precoder module is a 3D-GNN with attention mechanism.

A. Design of $f_H(\cdot)$

To learn $f_S(\cdot)$ and $f_P(\cdot)$, the loss function can be chosen as the negative objective function of problem P_N . To backpropagate the gradients of the loss function to the trainable weights in the scheduler module, the binary scheduling matrix **A** involved in $f_H(\cdot)$ as defined in (4) needs to be relaxed as a continuous variable during the training phase, and the function $f_H(\cdot)$ should be differentiable.

To this end, we realize $f_H(\cdot)$ by using basis vectors to extract the channels of scheduled users. Specifically, the matrix $\mathbf{A} \in \{0,1\}^{M \times K}$ is replaced by $\mathbf{B} \in \{0,1\}^{M \times K' \times K}$, whose mth slice is $\mathbf{B}_m \in \{0,1\}^{K' \times K}$. \mathbf{B}_m comprises K' different (row) basis vectors $\mathbf{b}_{m,k'} \in \{0,1\}^{1 \times K}, k' = 1, \cdots, K'$, satisfying $\sum_{k'=1}^{K'} \mathbf{b}_{m,k'} = \mathbf{a}_m$. There is a single "1" and K-1 "0"s in each vector $\mathbf{b}_{m,k'}$. $b_{m,k',k} \in \{0,1\}$ denotes the kth element in $\mathbf{b}_{m,k'}$.

Consequently, $f_H(\cdot)$ can be expressed as a slice-wise function. Specifically, the channels of the scheduled users on the mth RB, \mathbf{H}'_m , can be extracted by multiplying the basis vectors with \mathbf{H}_m as $\mathbf{H}'_m = (\mathbf{B}_m \otimes \mathbf{I}_{N_R})\mathbf{H}_m \in \mathbb{C}^{K'N_R \times N_T}$, which is the explicit expression of $f_H(\cdot)$ on the RB.

B. Graph Construction

To design GNNs with the same permutation properties as the two policies, two graphs are constructed as illustrated in Fig. 2. In the graphs, three types of vertices are defined corresponding to the three sets listed in Table I, including RB, $\mathrm{AN^{BS}}$, and $\mathrm{AN^{UE}}$ vertices, where the N_R $\mathrm{AN^{UE}}$ vertices at each user are referred to as a group of vertices.

Features are the input of GNNs. In both graphs, each element in the channel array \mathbf{H} or \mathbf{H}' is defined as a feature of a hyper-edge connecting one RB, one $\mathrm{AN^{BS}}$, and one $\mathrm{AN^{UE}}$ vertices, as illustrated in green in Fig. 2. For example, $(\mathbf{H})_{m,kr,n}$ is the feature of the hyper-edge connecting the mth RB, the nth $\mathrm{AN^{BS}}$, and the krth $\mathrm{AN^{UE}}$ vertices in Fig. 2(a).

Actions are the output of GNNs. An action is defined on vertices or edges. Specifically, in the scheduling graph, as illustrated in Fig. 2(a), each basis vector in ${\bf B}$ represents an action on an edge connecting an RB vertex and a group of ${\bf AN^{\rm UE}}$ vertices (shown in red). In the precoding graph, as illustrated in Fig. 2(b), each element in ${\bf v'_{RF}}$ is defined as an action on ${\bf AN^{\rm UE}}$ vertex (shown in orange), each vector in ${\bf W_{RF}}$ is defined as an action on ${\bf AN^{\rm BS}}$ vertex (shown in blue), and each vector in ${\bf W'_{BB}}$ is defined as an action on an edge between an RB vertex and a group of ${\bf AN^{\rm UE}}$ vertices (shown in pink).

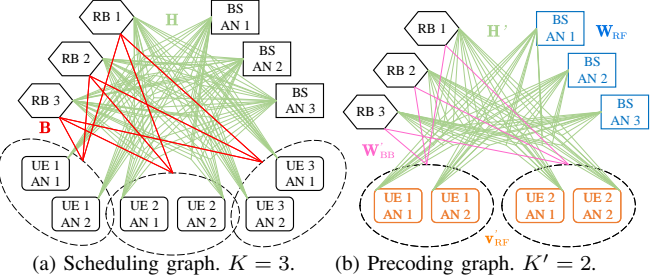


Fig. 2. Two constructed graphs. M = 3, $N_R = 2$, $N_T = 3$.

C. Design of Scheduler Module

To improve the learning performance of the scheduling policy, we define two model-based features that incorporate domain knowledge on the scheduling graph.

First, since scheduling largely depends on the strength of channels, the first model-based feature is defined as the channel strength

$$\bar{F}_{Sm,k} = ||\mathbf{H}_{m,k}||_F \in \mathbb{R}, \ \forall m, k.$$

This feature is associated with the edge connecting an RB vertex and a group of $AN^{\rm UE}$ vertices.

Second, the semi-orthogonal user selection (SUS) algorithm [28] suggests the importance of orthogonality between the channels of two users on each RB for scheduling. Considering the multiple antennas at each user, the second model-based feature is the averaged correlation coefficient between one channel vector and all others on an RB

$$\bar{F}_{\text{Om},kr} = \frac{1}{KN_R} \sum_{i=1}^{K} \sum_{n=1}^{N_R} \frac{|\mathbf{h}_{m,iu}^H \mathbf{h}_{m,kr}|}{||\mathbf{h}_{m,iu}||_2 ||\mathbf{h}_{m,kr}||_2} \in \mathbb{R}, \forall m, k, r,$$

This feature is associated with the edge connecting an RB vertex and an AN^{UE} vertex.

To enhance generalization performance and mitigate the impact of varying distributions of the two model-based features with respect to the number of transmit antennas N_T , receive antennas N_R , and candidate users K, we normalize the features as

$$F_{\text{S}m,k} = \frac{\bar{F}_{\text{S}m,k} - \text{mean}_{i \in \{1, \dots, K\}}(\bar{F}_{\text{S}m,i})}{\text{std}_{i \in \{1, \dots, K\}}(\bar{F}_{\text{S}m,i})},$$

$$F_{\text{O}m,kr} = \frac{\bar{F}_{\text{O}m,kr} - \text{mean}_{iu \in \{11, \dots, KN_R\}}(\bar{F}_{\text{O}m,iu})}{\text{std}_{iu \in \{11, \dots, KN_R\}}(\bar{F}_{\text{O}m,iu})}.$$

Based on the constructed graph, we design a 3D-GNN for the scheduler module. In the 3D-GNN, similar to the features \mathbf{H} , hidden representations are also defined on "hyperedges", which explains the "3D" designation [19]. In particular, $\mathbf{x}_{m,kr,n}^l \in \mathbb{R}^{C_l}$ denotes hidden representation of the hyperedge connecting the mth RB, the krth $\mathrm{AN^{UE}}$, and the nth $\mathrm{AN^{BS}}$ vertices in the lth layer, where $l=1,\cdots,L_S,\ L_S$ is the total number of layers of the GNN, and C_l is the number of elements in hidden representation of the lth layer.

The 3D-GNN comprises three key components: input, update, and output processes, which are introduced below.

- 1) <u>Input Process</u>: This process aims to generate all representations in the first layer from features. Each representation is given by $\mathbf{x}_{m,kr,n}^1 = [\mathrm{Re}((\mathbf{H})_{m,kr,n}), \mathrm{Im}((\mathbf{H})_{m,kr,n}), F_{\mathrm{S}m,k}, F_{\mathrm{O}m,kr}]^T \in \mathbb{R}^4$, which is associated with the corresponding hyper-edge as shown in Fig. 2(a).
- 2) <u>Update Process</u>: This process aims to update hidden representations layer by layer. Each representation is updated by aggregating the representations of its adjacent hyper-edges, which are the hyper-edges that differ from the updated one by only one index (i.e., in m, kr, or n). Four kinds of adjacent hyper-edges can be distinguished from the four subscripts. As analyzed in Sec. III-D, linear aggregators can enable the 3D-GNN to be generalized well to the sizes of all sets. Therefore, we use four trainable weights to linearly aggregate the representations of adjacent hyper-edges, and use another trainable weight to combine the updated representation itself. As visualized in Fig. 3, the update process can be expressed as

$$\mathbf{x}_{m,kr,n}^{l+1} = \phi \left(\mathbf{P}_1^l \mathbf{x}_{m,kr,n}^l + \mathbf{P}_2^l \frac{1}{M} \sum_{\substack{s=1\\s \neq m}}^M \mathbf{x}_{s,kr,n}^l + \mathbf{P}_3^l \frac{1}{KN_R} \right)$$

$$\sum_{\substack{l=1\\l\neq k}}^{K} \sum_{u=1}^{N_R} \mathbf{x}_{m,tu,n}^l + \mathbf{P}_4^l \frac{1}{N_R} \sum_{\substack{u=1\\u\neq r}}^{N_R} \mathbf{x}_{m,ku,n}^l + \mathbf{P}_5^l \frac{1}{N_T} \sum_{\substack{v=1\\v\neq r}}^{N_T} \mathbf{x}_{m,kr,v}^l \right),$$
(8)

where $\mathbf{P}_{j}^{l} \in \mathbb{R}^{C_{l+1} \times C_{l}}, \ j=1,\cdots,5$ are trainable weights and $\phi(\cdot)$ is an activation function.

3) <u>Output Process</u>: This process aims to produce action ${\bf B}$ from the hidden representations, whose size is $C_{LS}=1$, in the last layer, namely $x_{m,kr,n}^{LS}\in \mathbb{R}$. The representations are defined on hyper-edges, while the action is defined on edges. In other words, all representations compose a four-dimensional array ${\bf X}^{LS}\in \mathbb{R}^{M\times KN_R\times N_T\times C_{LS}}$, but all actions compose ${\bf B}\in\{0,1\}^{M\times K'\times K}$. Hence, we first compress the high-dimensional representation over N_T and N_R as

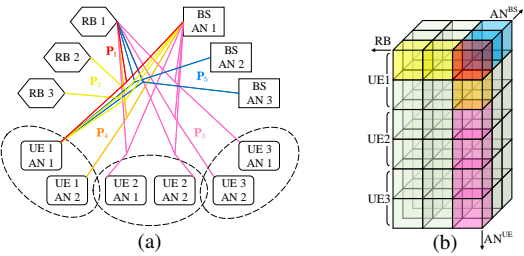


Fig. 3. Update process of 3D-GNN. $M=3, K=3, N_R=2, N_T=3$. In (a), the hidden representation of the red hyper-edge (with subscript m=k=r = n = 1) is updated by combining itself and the aggregated information from four kinds of adjacent hyper-edges. Different colors indicate different weights. In (b), each cube denotes a hyper-edge and its color is consistent

$$z_{m,k} = \frac{1}{N_R N_T} \sum_{r=1}^{N_R} \sum_{n=1}^{N_T} x_{m,kr,n}^{L_S} \in \mathbb{R}. \tag{9}$$
 With $z_{m,k}$, we can obtain the action $\mathbf B$ in both the testing and

training phases as follows.

Testing phase: For each RB, the K' basis vectors in \mathbf{B}_m are determined by the indices corresponding to the largest K'values in $z_{m,k}, k = 1, \dots, K$. In particular, the kth element in the k'th basis vector is given by $b_{m,k',k} = \text{Top}_{k'}(z_{m,k})$, where $\operatorname{Top}_{k'}(z_{m,k}) = 1$ if $z_{m,k}$ is the k'th largest value among the K scalars $z_{m,k}, k=1,\cdots,K$, and $\operatorname{Top}_{k'}(z_{m,k})=0$ otherwise.

In this way, constraint (2) is satisfied since K' different basis vectors are provided on each RB.

Training phase: To enable back-propagation of gradients, K' basis vectors need to be relaxed as continuous vectors. To this end, we introduce the function $SoftTop_{k'}(\cdot)$ [29], which yields K' relaxed basis vectors $\tilde{\mathbf{b}}_{m,k'} \in (0,1)^{1\times K}$ one by one based on the values of $z_{m,k}, k = 1, \dots, K$. Specifically, for k' = 1, each element in the first relaxed basis vector is given by $\tilde{b}_{m,1,k} = \operatorname{Softmax}_{\tau}(z_{m,k}) = \exp(z_{m,k}/\tau)/(\sum_{i=1}^K \exp(z_{m,i}/\tau))$, where $\operatorname{Softmax}_{\tau}(\cdot)$ is a temperature-parameterized function that generates a probability, and $\tau > 0$ is the temperature controlling the smoothness of the output distribution. As the training epochs increase, the values of τ decrease, making the distribution more concentrated and close to the discretized results. This approach reduces the discrepancy between the outcomes during training and testing phases.

Next, for each k' > 1, the values of $z_{m,k}, k = 1, \dots, K$ are adjusted based on the probability obtained in the previous round as $z_{m,k}^{(k')} = z_{m,k}^{(k'-1)} + \log(1 - \tilde{b}_{m,k'-1,k})$, where $z_{m,k}^{(1)} = z_{m,k}$. Then, the k'th relaxed basis vector is represented by $\tilde{b}_{m,k',k} = \operatorname{Softmax}_{\tau}(z_{m,k}^{(k')})$. After K' rounds of this process, we can obtain K' relaxed basis vectors on each RB.

4) A Sequence of GNNs to Enhance Scheduler Module: As mentioned in Sec. III-D, a single GNN cannot well learn the non-SPSD scheduling policy in the scenario with densely distributed users. To address it, we design a scheduler module consisting of K' 3D-GNNs, as shown in Fig. 4.

The idea is to let each GNN merely choose a single user on every RB, i.e., the k'th GNN generates basis vectors $\mathbf{b}_{m,k'}$, $m=1,\cdots,M$. Meanwhile, each subsequent GNN inputs not only the original features but also all the basis vectors generated by the preceding GNNs. This design ensures that once one user is scheduled, particularly the one with similar channels to

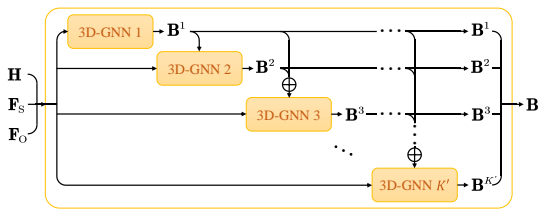


Fig. 4. A sequence of GNNs. They can replace the 3D-GNN in the scheduler module of NGNN as an enhancement. After the replacement, the whole architecture is referred to as SGNN.

others, the inputs to the subsequent GNNs become different. This method effectively reduces the similarity of inputs for one GNN, thereby avoiding performance degradation for learning non-SPSD policy.

Similar to the GNN designed in Sec. IV-C, herein each GNN also includes the input, update, and output processes. The update process is similar to that described in Sec. IV-C2 but with different trainable weights. We next briefly introduce

the other two processes. Input process: Let $\mathbf{x}_{m,kr,n}^{k',1} \in \mathbb{R}^{C_1}$ denote the first-layer representation of a hyper-edge connecting the mth RB, the krth AN^{UE}, and the nth AN^{BS} vertices for the k'th GNN. For the first GNN, $\mathbf{x}_{m,kr,n}^{1,1} = [\operatorname{Re}((\mathbf{H})_{m,kr,n}), \operatorname{Im}((\mathbf{H})_{m,kr,n}),$ $F_{\mathrm{S}m,k}, F_{\mathrm{O}m,kr}]^T \in \mathbb{R}^4$. For the subsequent GNNs, the inputs further include the summation of outputs from preceding GNNs. Specifically, the input for the k'th GNN is $\mathbf{x}_{m,kr,n}^{k',1} = [\operatorname{Re}((\mathbf{H})_{m,kr,n}), \operatorname{Im}((\mathbf{H})_{m,kr,n}), F_{Sm,k}, F_{Om,kr},$ $\sum_{j=1}^{k'-1} b_{m,j,k}]^T \in \mathbb{R}^5, \ k' = 2, \cdots, K'.$

Output process: Each GNN generates a basis vector for every RB. For the k'th GNN, like in (9), the hidden representation in the last layer $x_{m,kr,n}^{k',L_S} \in \mathbb{R}$ is first compressed as $z_{m,k}^{k'} = \sum_{r=1}^{N_R} \sum_{n=1}^{N_T} \frac{z_{m,kr,n}^{k',L_S}}{N_R N_T} / N_R N_T \in \mathbb{R}$. With $z_{m,k}^{k'}$, in the testing phase, the kth element in the basis vector is discretized by $b_{m,k',k}=\operatorname{Onehot}(z_{m,k}^{k'})$, where $\operatorname{Onehot}(z_{m,k}^{k'})=1$ if $z_{m,k}^{k'}\geq z_{m,i}^{k'}$ for $\forall i\in\{1,\cdots,K\}$, and $\operatorname{Onehot}(z_{m,k}^{k'})=0$ otherwise. In Fig. 4, the M basis vectors yielded by the k'th GNN compose a matrix $\mathbf{B}^{k'} \in \{0,1\}^{M \times K}$. In the training phase, the relaxed basis vector is given by $\tilde{b}_{m,k',k} =$ $\operatorname{Softmax}_{\tau}(z_{m,k}^{k'}).$

By introducing the sequence of GNNs, each employing a discretization step, the scheduler module learns a noncontinuous function that produces very different outcomes for users with similar channels. After jointly training with the precoder module to maximize SE, the K' GNNs will schedule different users on the same RB, ensuring that constraint (2) is satisfied with high probability.

Although SGNN is designed for scenarios with dense user population, it can also be applied in other scenarios, albeit with higher complexity compared to NGNN.

D. Design of Precoder Module

As discussed in Sec. III-D, the precoding policy is SPSD on ANBS, AN, and RB sets, but non-SPSD on user set. It indicates that GNNs are not generalizable to the number of users without a judicious design, even if they are permutation equivariant to users.

Inspired by the design in [18, 19] for precoding in narrowband MU-MISO systems, the generalization performance to varying K can be improved by weighting the information before aggregation, where the weights can reflect the strength of MUI. We propose an attention coefficient for precoding in wideband MU-MIMO systems. Different from [18, 19], the attention coefficient is computed on each RB and needs to reflect the total MUI on multiple receive antennas at users.

The precoder module is an L_P -layer 3D-GNN, where the hidden representation of the hyper-edge connecting the mth RB, the k'rth AN^{UE}, and the nth AN^{BS} in the lth layer is denoted as $\mathbf{y}_{m,k'r,n}^l \in \mathbb{R}^{D_l}$, $l=1,\cdots,L_P$. We next introduce the input process, update process with a partial attention mechanism, and output process of the GNN.

- 1) Input Process: The representations in the first layer are the channels of scheduled users defined on the hyper-edges, as shown in Fig. 2(b). Each representation is expressed in the real-valued form as $\mathbf{y}_{m,k'r,n}^1 =$ $[\operatorname{Re}((\mathbf{H}')_{m,k'r,n}), \operatorname{Im}((\mathbf{H}')_{m,k'r,n})]^T \in \mathbb{R}^2.$
- 2) Update Process with Attention Mechanism: To enable the generalizability to the number of users K, we introduce an attention coefficient $\alpha_{m,t \to k'}^l \in \mathbb{R}^{D_{l+1}}$ to measure the MUI strength from the tth user to the k'th user on the mth RB. $\alpha_{m,t\to k'}^l$ is then multiplied on the aggregated representations connecting the antennas at the tth user. The other three kinds of representations of adjacent hyper-edges corresponding to the sets of RBs and antennas at both BS and users are aggregated linearly, which enables the generalizability due to the aforementioned SPSD property. As visualized in Fig. 5, the hidden representation of each hyper-edge in the (l+1)th

$$\mathbf{y}_{m,k'r,n}^{l+1} = \phi \left(\mathbf{Q}_{1}^{l} \mathbf{y}_{m,k'r,n}^{l} + \mathbf{Q}_{2}^{l} \frac{1}{M} \sum_{\substack{s=1\\s \neq m}}^{M} \mathbf{y}_{s,k'r,n}^{l} + \frac{1}{K'} \sum_{\substack{t=1\\t \neq k'}}^{K'} \boldsymbol{\alpha}_{m,t \to k'}^{l} \odot \mathbf{Q}_{3}^{l} \frac{1}{N_{R}} \sum_{u=1}^{N_{R}} \mathbf{y}_{m,tu,n}^{l} \quad (10) + \mathbf{Q}_{4}^{l} \frac{1}{N_{R}} \sum_{\substack{u=1\\u \neq r}}^{N_{R}} \mathbf{y}_{m,k'u,n}^{l} + \mathbf{Q}_{5}^{l} \frac{1}{N_{T}} \sum_{\substack{v=1\\v \neq n}}^{N_{T}} \mathbf{y}_{m,k'r,v}^{l} \right),$$

where the attention coefficient is obtained as

$$\boldsymbol{\alpha}_{m,t\to k'}^{l} = \tanh\left(\frac{1}{N_T} \sum_{v=1}^{N_T} \left(\mathbf{Q}_6^l \frac{1}{N_R} \sum_{u=1}^{N_R} \mathbf{y}_{m,tu,v}^l \right.\right.$$
$$\odot \mathbf{Q}_7^l \frac{1}{N_R} \sum_{v=1}^{N_R} \mathbf{y}_{m,k'u,v}^l\right), \qquad (11)$$

 $\mathbf{Q}_{j}^{l} \in \mathbb{R}^{D_{l+1} \times D_{l}}, \ j = 1, \cdots, 7$ are trainable weights, and $tanh(\cdot)$ is introduced to restrict the value of attention coefficient for assisting the generalization to the number of antennas.

If $\mathbf{Q}_6^1 = \mathbf{Q}_7^1 = \mathbf{I}$ and $N_R = 1$ in (11), the outer-layer summation over N_T in the first layer is the inner product between the channels of the tth and k'th users, whose value increases with the correlation between the channels. Since each user receives a single data stream, the attention coefficient between the averaged representations of the hyper-edges connecting two users over their receive antennas can be regarded as the total interference between them on an RB. With the aid of such attention coefficients, the importance of the information from different users on the hidden representation of a certain user can be well distinguished.

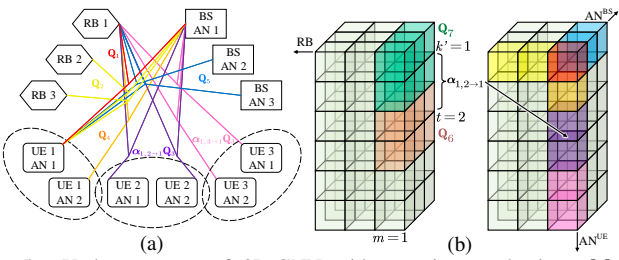


Fig. 5. Update process of 3D-GNN with attention mechanism. M = $3, K' = 3, N_R = 2, N_T = 3$. In (a), the hidden representation of the red hyper-edge (with subscript m = k' = r = n = 1) is updated. The aggregated information from different users are weighted differently. In (b), the computation of an attention coefficient is illustrated.

3) Output Process: The actions of the analog combiner and hybrid precoders are obtained from the hidden representations in the last layer after normalized to satisfy constraints. The number of elements in each $\mathbf{y}_{m,k'r,n}^{L_P}$ is set to $D_{L_P} = 4N_{\rm RF} + 2$.

The real and imaginary parts of $\tilde{\mathbf{W}}_{RF}$ come from the first and second N_{RF} elements, which are respectively

$$\text{Re}((\tilde{\mathbf{W}}_{\text{RF}})_{n,j}) = \frac{1}{MKN_R} \sum_{m=1}^{M} \sum_{k'=1}^{K} \sum_{r=1}^{N_R} (\mathbf{y}_{m,k'r,n}^{L_P})_j \in \mathbb{R},$$

$$\text{Im}((\tilde{\mathbf{W}}_{\text{RF}})_{n,j}) = \frac{1}{MKN_R} \sum_{m=1}^{M} \sum_{k'=1}^{K} \sum_{r=1}^{N_R} (\mathbf{y}_{m,k'r,n}^{L_P})_{N_{\text{RF}}+j} \in \mathbb{R},$$

$$\text{for } j = 1, \dots, N_{\text{RF}}. \text{ Then, to satisfy constraint (1b), }$$

$$(\mathbf{W}_{\text{RF}})_{n,j} = (\tilde{\mathbf{W}}_{\text{RF}})_{n,j} / |(\tilde{\mathbf{W}}_{\text{RF}})_{n,j}|.$$

The real and imaginary parts of $\tilde{\mathbf{W}}_{BB}'$ come from the third and fourth $N_{\rm RF}$ elements, which are respectively

$$\operatorname{Re}((\tilde{\mathbf{W}}'_{\mathrm{BB}})_{m,j,k'}) = \frac{1}{N_R N_T} \sum_{r=1}^{N_R} \sum_{n=1}^{N_T} (\mathbf{y}_{m,k'r,n}^{L_P})_{2N_{\mathrm{RF}}+j} \in \mathbb{R}$$
$$\operatorname{Im}((\tilde{\mathbf{W}}'_{\mathrm{BB}})_{m,j,k'}) = \frac{1}{N_R N_T} \sum_{r=1}^{N_R} \sum_{n=1}^{N_T} (\mathbf{y}_{m,k'r,n}^{L_P})_{3N_{\mathrm{RF}}+j} \in \mathbb{R},$$

for $j=1,\ldots,N_{\mathrm{RF}}$. Then, to satisfy power constraint (7a), $\mathbf{w}_{\mathrm{BB}m,k'}'=\tilde{\mathbf{w}}_{\mathrm{BB}m,k}'\sqrt{P_{tot}/\sum_{m=1}^{M}\sum_{k'=1}^{K'}||\mathbf{W}_{\mathrm{RF}}\tilde{\mathbf{w}}_{\mathrm{BB}m,k'}'||_{2}^{2}}$. The real and imaginary parts of $\tilde{\mathbf{v}}_{\mathrm{RF}}'$ come from the last two

elements, which are respectively

Re
$$((\tilde{\mathbf{v}}_{\mathrm{RF}}')_{k'r}) = \frac{1}{MN_T} \sum_{m=1}^{M} \sum_{n=1}^{N_T} (\mathbf{y}_{m,k'r,n}^{L_P})_{4N_{\mathrm{RF}}+1} \in \mathbb{R}$$

$$\mathrm{Im}((\tilde{\mathbf{v}}_{\mathrm{RF}}')_{k'r}) = \frac{1}{MN_T} \sum_{m=1}^{M} \sum_{n=1}^{N_T} (\mathbf{y}_{m,k'r,n}^{L_P})_{4N_{\mathrm{RF}}+2} \in \mathbb{R},$$
when, to satisfy constraint (7b), $(\mathbf{v}_{\mathrm{RF}}')_{k'r}$

Then, to satisfy $(\tilde{\mathbf{v}}'_{RF})_{k'r}/|(\tilde{\mathbf{v}}'_{RF})_{k'r}|.$

Remark 1: The proposed architecture can be extended to the setup where each user receives $N_S > 1$ data streams, and both data streams and users need to be selected [5]. In this case, the scheduling matrix becomes $\mathbf{A} \in \{0,1\}^{M \times KN_S}$ and its version with basis vectors becomes $\mathbf{B} \in \{0, 1\}^{M \times N_D \times KN_S}$, where N_D is the total number of data streams. The number of scheduled users K' ranges from $[N_D/N_S]$ to N_D , where [.] stands for the ceiling operation. For the GNNs in the two modules, the weight-sharing and attention mechanism should be designed by taking the permutation of data streams into consideration [19], where the design of attention mechanism remains an open problem.

E. Training Phase and Test Phase

Next, we show how to train the architecture (including NGNN and SGNN) and apply it for inference.

- 1) Training Phase: The precoder module should be adaptable to different channel distributions of the scheduled users, meanwhile the performance of a scheduler depends on the precoder. Moreover, an adequate precoder is a prerequisite for training the scheduler. If a random precoder is used, then the scheduler cannot find the users to maximize the SE. Hence, the precoder module should be pre-trained first, and then fine-tuned by jointly training the two modules.
- a) Training the Precoder Module: To allow the GNN in the precoder module to fast adapt to channel distribution determined by the scheduler module, the GNN is pre-trained by the samples each comprising the channels of K' users selected from K users by a simple scheduling method, i.e., choosing K' users with the strongest channels on each RB.

The loss function for one sample is $\mathcal{L} = -\frac{1}{M} \sum_{m=1}^{M} \sum_{k'=1}^{K'} R'_{m,k'}$. Then, the gradient of the averaged loss over a batch of samples is back-propagated to update the trainable weights in the GNN.

- b) Training the Scheduler Module: The scheduler module is trained by the samples each with the channels of K candidate users. These samples go through the entire architecture, composed of the trainable scheduler and the pretrained precoder with frozen weights. The loss function is also \mathcal{L} , but the scheduled users may change during training. The gradient of the averaged loss over a batch of samples is backpropagated to update the weights in the GNN (or GNNs) in the scheduler module.
- c) Jointly Training the Two Modules: The two modules are trained jointly by the same samples as those for training the scheduler module. These samples go through the entire architecture, where the weights of all GNNs in both modules have been pre-trained. The loss function remains \mathcal{L} . The gradient of the averaged loss over a batch of samples is backpropagated to fine-tune the weights in all GNNs.
- 2) Test Phase: If K > K', the inference process is shown in Fig. 1. The scheduler module yields scheduling outcome, and the precoder module produces the corresponding combiner and precoders. If $K \le K'$, the scheduler module is inactive, and the combiner and precoders can be obtained from the precoder module with $\mathbf{H}' = \mathbf{H}$.

Since the number of weights in the designed GNNs is independent of the graph sizes, the well-trained architecture can be applied to different numbers of RBs, candidate users, and antennas at the BS and each user during the test phase.

F. Computational Complexity Analysis

The computational complexity for inference is measured in floating point operations (FLOPs).

1) 3D-GNN in Scheduler Module: The one in NGNN and each one in SGNN have the same expression of complexity but with different hyper-parameters. We analyze the update process in Sec. IV-C2, because the complexities of input and output processes are ignorable. In the first term on the right-hand side of (8), multiplying the matrix by a vector requires $C_{l+1}C_l$ multiplications and $C_{l+1}(C_l-1)$ additions. This term

needs to be computed for all the MKN_RN_T hyper-edges. The second term can be rewritten as $\tilde{\mathbf{P}}_{2\,\overline{M}}^l\sum_{s=1}^M\mathbf{x}_{s,kr,n}^l$ such that it can be reused across RBs, where $C_{l+1}(C_l+1)$ multiplications and $C_{l+1}(C_l-1)+C_l(M-1)$ additions are required. This term needs to be computed KN_RN_T times for all hyperedges. The FLOPs for the other three terms can be derived similarly, and the sum of five terms involves $4C_{l+1}$ additions. Thereby, the total FLOPs required by one layer of a 3D-GNN in the scheduler module is $C_{l+1}(2C_l-1)MKN_RN_T+2C_{l+1}C_l(KN_RN_T+MN_T+MKN_T+MKN_T)+C_l[(M-1)KN_RN_T+(KN_R-1)MN_T+(N_R-1)MKN_T+(N_T-1)MKN_R]+4C_{l+1}$. The overall complexity of SGNN is higher than that of NGNN because SGNN employs K' 3D-GNNs in the scheduler module.

2) 3D-GNN in Precoder Module: It is same for both the NGNN and SGNN. Except the third term in (10), the update process is analogous to (8). The attention coefficient in (11) is realized by two matrix-vector multiplications and a matrix-matrix (with sizes of $K' \times N_T$ and $N_T \times K'$) multiplication. Then, to incorporate attention coefficient, the third term needs a matrix-vector multiplication and a matrix-matrix (with sizes of $K' \times K'$ and $K' \times N_T$) multiplication. Thereby, the total FLOPs required by one layer of the 3D-GNN in the precoder module is $D_{l+1}(2D_l-1)MK'N_RN_T+2D_{l+1}D_l(K'N_RN_T+4MK'N_T+MK'N_R)+D_l[(M-1)K'N_RN_T+(N_R-1)MK'N_T+(N_T-1)MK'N_R]+D_{l+1}MN_T(4K'^2+4K'N_R-K'+1).$

The order of magnitude of FLOPs for the scheduler and precoder modules in the proposed architecture, including both the NGNN and SGNN, are provided in Table II, where $C_{l+1} = C_l = C$ and $D_{l+1} = D_l = D$ are assumed for notational simplicity. For comparison, we also list the results of several numerical algorithms for wideband scheduling, wideband hybrid precoding, or joint designing the two, where C_{pre} represents the complexity of the used precoding algorithm. It is evident that both modules in the proposed architecture are with the lowest complexity (except the "Strongest" scheduling) due to the lack of high-order terms of N_T and N_R .

TABLE II COMPUTATIONAL COMPLEXITY

| Scheduling Methods | Asymptotic Complexity | | | |
|-----------------------|--|--|--|--|
| Scheduler in NGNN | $O(MKN_RN_TL_SC^2)$ | | | |
| Scheduler in SGNN | $O(MKK'N_RN_TL_SC^2)$ | | | |
| Multicarrier SUS [30] | $O(MKK'N_R^2N_T^2)$ | | | |
| Strongest | $O(MK(N_RN_T + \log K'))$ | | | |
| Precoding Methods | Asymptotic Complexity | | | |
| Precoder in NGNN/SGNN | $O(MK'N_RN_TL_PD(K'+D))$ | | | |
| SDR | $O(MK'^2N_{RF} + MK'N_{RF}^2 + N_T^{4.5})$ | | | |
| MO [31] | $O(MN_T^2N_{RF} + MN_TN_{RF}^2 + MN_{RF}^3)$ | | | |
| OMP [26] | $O(MK'^2N_{RF}N_T^2 + K'N_R^2)$ | | | |
| SVD [26] | $O(MK'^3N_{RF}N_T + K'N_R^2)$ | | | |
| EIG [32] | $O(MK'^3 + MK'N_{RF}N_T + N_{RF}N_T^2)$ | | | |
| Joint Methods | Asymptotic Complexity | | | |
| Exhaustive | $O({K \choose K'}^M C_{pre})$ | | | |
| Greedy | $O(MKK'C_{pre})$ | | | |
| LISA [5] | $O(MKN_R^2N_T + K\min(M^2N_T, MN_T^2) + r^3)$ rank of channels $r \le \min(MN_R, N_T)$ | | | |

SDR: semidefinite relaxation [7], MO: manifold optimization [3], OMP: orthogonal matching pursuit [33], SVD: singular value decomposition [26], EIG: eigen-decomposition [32].

Besides, if the channel of each user is regarded as a token or a feature of a user vertex, we can show that the dominant term in the number of FLOPs required by Transformer [12] and GAT [24] is $O(K'^2)$. This indicates that their computational complexities are comparable to the GNN in the precoder module. The dominant term will be $O(K^2)$ if the joint policy $f_J(\cdot)$ is learned, since the features and actions are considered for all candidate users including the unscheduled ones.

V. SIMULATION RESULTS

In this section, we evaluate the learning performance, size generalizability, inference and training complexities of the two variants of the proposed architecture: NGNN and SGNN.

Consider a non-line-of-sight channel model in urban macro (UMa) scenario [34]. The system and channel parameters are listed in Table III. Users are randomly located in a sector of a cell. Both BS and users are equipped with uniform planar array. Each RB consists of 12 subcarriers and 14 OFDM symbols in a time slot. The noise power on each RB is $\sigma^2 = P_n/M_{max}$, where the noise power in the entire bandwidth $P_n(\mathrm{dBm}) = N_0 + 10\log_{10}(BW) + N_F$. The pathloss model is $PL(\mathrm{dB}) = 13.54 + 39.08\log_{10}(d_{3D}) + 20\log_{10}(f_c(\mathrm{GHz})) - 0.6(h_U - 1.5)$ [34], where d_{3D} is the distance between user and BS. The maximal number of scheduled users is $K' = N_{\mathrm{RF}}$.

| TABLE III | |
|------------------|---|
| SIMULATION SETUE |) |

| Description | Notation | Value | |
|--------------------------------------|-------------|--------------|--|
| Carrier frequency | f_c | 28 GHz | |
| Bandwidth | BW | 400 MHz | |
| Subcarrier spacing | - | 120 kHz | |
| Maximal number of RBs | M_{max} | 264 | |
| Default transmit power | P_{tot} | 46 dBm | |
| Noise spectral density | N_0 | -174 dBm/Hz | |
| Noise figure | N_F | 7 dB | |
| Number of candidate users | K | 1 to 60 | |
| Number of antennas at the BS | N_T | 8 to 128 | |
| Number of RF chains at the BS | $N_{ m RF}$ | 2 to 12 | |
| Height of BS antennas | - | 25 m | |
| Number of antennas at each user | N_R | 1 to 8 | |
| Height of user antennas | h_U | 1.5 to 2.5 m | |
| Cell radius | - | 250 m | |
| Minimum distance between BS and user | - | 35 m | |
| User velocity | - 3 km/h | | |
| Standard deviation of shadowing | - | 6 dB | |

We generate 200,000 samples for training and 2,000 samples for testing the DNNs. Activation function is $ReLU(\cdot)$, optimizer is Adam, and batch normalization is used. The tuned hyper-parameters are as follows. The batch-size is 50. Initial learning rates are 0.001 and 0.0003 for the precoder and scheduler modules, respectively. The numbers of elements in hidden representations are [4, 64, 64, 64, 64, 1] for the six layers in the GNN for scheduling in NGNN, [5, 32, 32, 1] for the four layers in each GNN in the scheduler module of SGNN, and [2, 128, 128, 128, 128, 128, 128, $2+4N_{RF}$ for the eight layers in the GNN for precoding in both variants. The numbers of epochs for training the precoder module, scheduler module, and jointly training the two modules are $E_P = 90$, $E_S = 10$, and $E_J = 100$, respectively. The temperature parameter decays according to $\tau = 0.1 + 0.4 \exp(-0.02 \times \text{epoch}).$

A. Learning Performance

We first evaluate the SE achieved by NGNN and SGNN, by comparing with three numerical algorithms for wideband scheduling and hybrid precoding: LISA [5], Greedy [6], and SDR [7]. "LISA" and "Greedy" jointly design scheduling and precoding, where ZF constraint is imposed on precoders in "LISA" and ZF precoder is employed when selecting users in "Greedy". "SDR" only optimizes precoding, where the users with strongest channels are scheduled. Since few studies jointly design scheduling and precoding, we further simulate four precoding-only algorithms: SVD [26], EIG [32], MO [3], and OMP [33], which are used together with a multicarrier SUS [30] scheduling algorithm.

In Fig. 6, we show the impact of signal-to-noise ratio (SNR). In Fig. 6(a), each user is with a single antenna. It is shown that NGNN and SGNN perform closely to "SDR" and outperform other methods. The gap between NGNN and SGNN is minor, because the impact of the non-SPSD property of the scheduling policy is negligible in the considered UMa scenario.

In the sequel, "SDR", "Greedy", and "EIG" are no longer simulated, since they are designed for single-antenna users. "MO" and "OMP" are also not simulated anymore, due to their time-consuming iterations and inferior performance. To obtain a benchmark for comparison, we develop an integrated method "LISA-SDR", whose scheduling algorithm and analog combiner come from "LISA" and precoders come from "SDR" based on the equivalent channel, i.e., multiplied by the analog combiner. Besides, the following three learning-based methods are compared:

- GAT: All 3D-GNNs in the SGNN are replaced by GATs, which learn over graphs with only user vertices [22].
- CNN: Two CNNs, each composed of convolutional layers with kernel size of 3 × 3 and a fully connected layer [35], serve as the scheduler and precoder modules.
- FNN: Two FNNs serve as the scheduler and precoder modules.

In Fig. 6(b), each user is with two antennas. The superior performance of NGNN and SGNN is evident from the enlarged gaps with other learning methods as SNR increases. GAT performs poor owing to its failure to distinguish MUI with properly designed attention mechanism and to leverage the permutation priors of antennas and RBs. CNN and FNN cannot harness any permutation prior and then perform worse.

In Fig. 7, we show the impact of the number of RF chains when $P_{tot} = 46$ dBm. The result is similar to that in Fig. 6(b).

In Fig. 8, we show the gain of the sequential design in SGNN. To this end, we consider a scenario with crowded candidate users, which are located in a $10\times10~\text{m}^2$ area at 100 m away from the BS. The channels are generated according to the clustered delay line-A model [34]. It shows that SGNN outperforms NGNN more evidently as N_{RF} increases, since NGNN cannot properly select users with similar channels. Besides, both SGNN and NGNN achieve higher SE than other methods.

B. Generalizability to Unseen Problem Scales

Next, we assess the generalizability of well-trained DNNs, by the ratio of the SE achieved by the learned policies

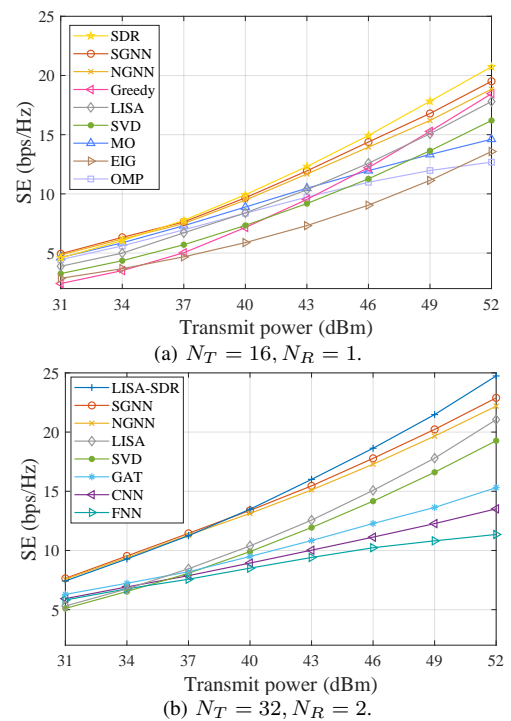


Fig. 6. Impact of P_{tot} , M = 16, K = 10, $N_{RF} = 4$.

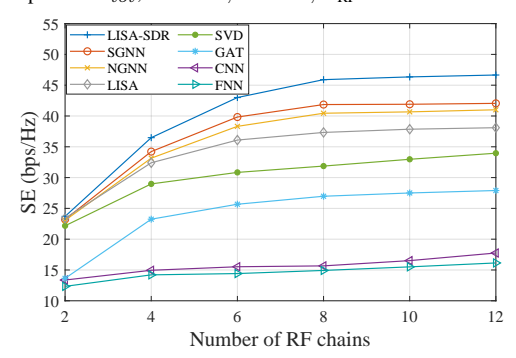


Fig. 7. Impact of N_{RF} , M = 4, K = 30, $N_T = 32$, $N_R = 2$.

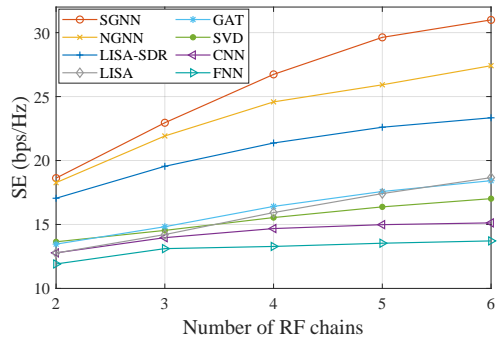


Fig. 8. Impact of scenario, $M = 16, K = 30, N_T = 16, N_R = 2$.

to the SE achieved by "LISA-SDR", which can serve as a performance upper bound in the UMa scenario. We also provide the results of "LISA" [5] and "SVD" [26], which are simulated for every value of M, K, N_T , or N_R .

According to previous analyses, NGNN and SGNN can be generalized to the numbers of RBs, users, $AN^{\rm BS}s$, and $AN^{\rm UE}s$. GAT is generalizable to the number of users, but CNN and FNN are not generalizable to any problem scales. To show the impacts of the model-based features and attention mechanism, two modified SGNNs are also simulated: "SGNN w/o F" (that

is an SGNN without the model-based features in the scheduler module), and "SGNN w/o A" (that is an SGNN without the attention coefficient in the precoder module).

In Fig. 9, we provide the SE ratios achieved by the GNNs that are trained with samples of 16 RBs and tested with samples of 4 to 128 RBs without re-training. As expected, all GNNs can be well generalized to the number of RBs. The performance of "LISA" and "SVD" degrades with the enlarged bandwidth, because they involve the matrix factorization of the summation or concatenation of channels across different RBs.

In Fig. 10, we provide the SE ratios achieved by the GNNs that are trained with samples of 30 candidate users, and tested with samples of 3 to 60 users. When $K \leq N_{\rm RF}$, the generalizability of the precoder module is examined since the scheduler module is inactive. We can see that the proposed attention mechanism significantly improves generalization performance. When $K > N_{\rm RF}$, the generalizability of the scheduler module is evaluated since precoder always serves $N_{\rm RF}$ users. We can see that "SGNN w/o F" performs worse than SGNN when K is large, which indicates the benefit of model-based features for size generalization of scheduling.

In Fig. 11, we provide the SE ratios achieved by the GNNs that are trained with samples of 16 antennas at the BS and tested with samples of 8 to 128 antennas. In Fig. 12, the GNNs are trained with $N_R=4$ and tested with one to eight antennas. In both figures, all GNNs can be well generalized, except "SGNN w/o F", which has a slight decline attributed to the changing channel distribution with N_T and N_R .

It is noteworthy that the favorable generalization performance to the numbers of RBs, candidate users (for scheduling), $AN^{\rm BS}$ s, and $AN^{\rm UE}$ s is achieved only with linear aggregators, as shown in the update equation in (8) and (10). This validates our observation in Sec. II-B.

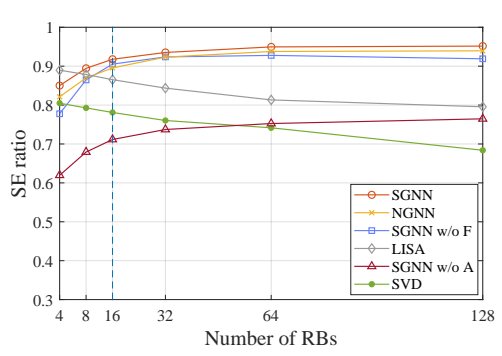


Fig. 9. Generalizability to M, K=20, $N_{\rm RF}=4$, $N_T=16$, $N_R=2$.

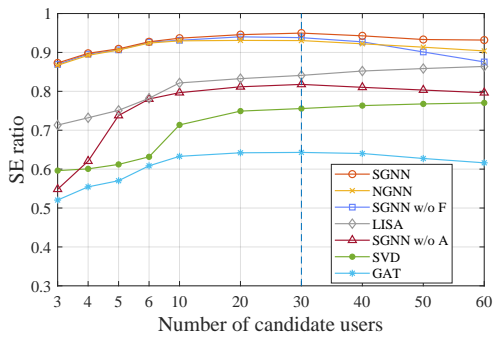


Fig. 10. Generalizability to K, M = 16, $N_{RF} = 6$, $N_T = 16$, $N_R = 2$.

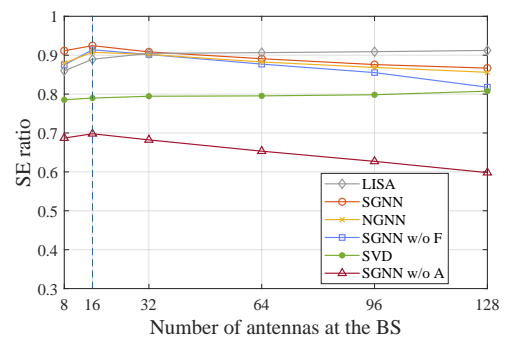


Fig. 11. Generalizability to N_T , M=4, K=20, $N_{RF}=4$, $N_R=2$.

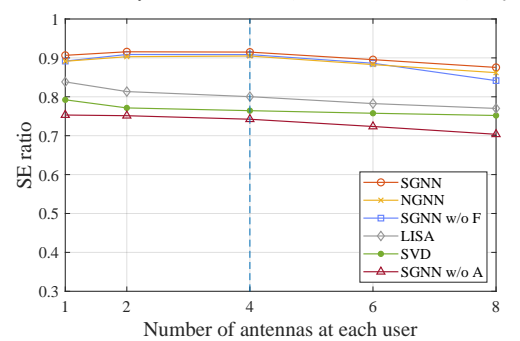


Fig. 12. Generalizability to N_R , M=16, K=20, $N_{RF}=4$, $N_T=16$.

C. Inference Complexity and Training Complexity

Finally, we evaluate the inference and training complexities of the learning-based methods, which determine the required computing resources in practical applications.

In Table IV, we list the inference complexities of the GNNs that can achieve comparable performance as "LISA-SDR" in Fig. 10, where the time complexity refers to the runtime for inference and the space complexity refers to the number of trainable weights. Since numerical algorithms can only run on CPU, the time complexity is obtained on an Intel Core i9-10940X CPU for a fair comparison. We can see that "LISA-SDR" requires long time for convergence, whereas NGNN and SGNN are $50 \sim 100$ times faster. The storage demand of the trainable weights in a GNN is about 2.4 M bytes if single-precision floating-point format is used.

 $\begin{array}{c} \text{TABLE IV} \\ \text{Inference Complexity } (M=16, N_{\text{RF}}=6, N_T=16, N_R=2) \end{array}$

| | K | NGNN | SGNN | SGNN w/o F | LISA-SDR |
|------------------|----|------|------|------------|----------|
| Time complexity | 20 | 81 | 101 | 98 | 8927 |
| (ms) | 40 | 98 | 155 | 150 | 9058 |
| (1115) | 60 | 112 | 179 | 173 | 9205 |
| Space complexity | - | 662k | 635k | 633k | - |

In Fig. 13, we depict the runtime of different methods. It can be seen that the runtime of "LISA" and "SVD" are comparable to those of the GNNs, yet their performance are inferior as demonstrated in Figs. $6\sim12$.

In Fig. 14, we provide the SE ratio achieved by the DNNs trained with different numbers of samples. It is shown that SGNN and NGNN outperform other DNNs. CNN and FNN allocate the majority of power to a single user on an RB, whose performance grows slowly. This also explains why their performance hardly increases with $N_{\rm RF}$ in Fig. 7. GAT surpasses CNN and FNN, but the gap between it to the proposed methods is significant.

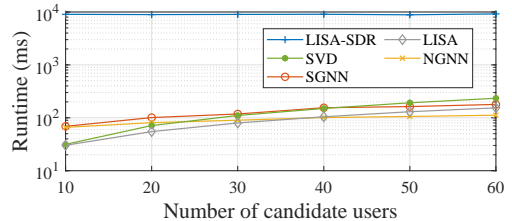


Fig. 13. Runtime versus $K, M = 16, N_{RF} = 6, N_T = 16, N_R = 2$.

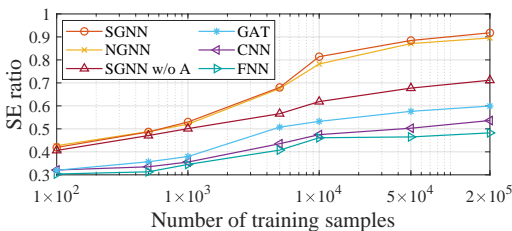


Fig. 14. Impact of the number of training samples, $M=16, K=20, N_{\rm RF}=4, N_T=16, N_R=2.$

In Table V, we provide the training complexities of different DNNs, where the two values before and after the slash are respectively for the scheduler and precoder modules. The space, sample, and time complexities indicate the minimal requirements of trainable weights, training samples, and training time to achieve an expected performance. To enable all DNNs to achieve the same performance, a narrow-band system is considered, and the performance is set as 85% SE of "LISA-SDR". The DNNs are trained on NVIDIA GeForce RTX 3080 GPU. It is observed that the training complexity of NGNN and SGNN are lower than other DNNs, owing to exploiting permutation priors and introducing the attention mechanism.

 $\begin{array}{c} {\rm TABLE~V} \\ {\rm Training~Complexity} \\ (M=1,K=10,N_{\rm RF}=4,N_T=16,N_R=1,P_{tot}=40{\rm dBm}) \end{array}$

| Methods | NGNN | SGNN | GAT | CNN | FNN |
|-----------------------------------|--------|--------|--------|---------|-----------|
| Number of layers | 6/6 | 4/6 | 4/6 | 6/6 | 6/8 |
| Elements in hidden representation | 32/128 | 16/128 | 64/256 | 128/256 | 1024/2048 |
| Space complexity | 374k | 369k | 2.26M | 5.73M | 25.1M |
| Sample complexity | 4.0k | 3.3k | 380k | 900k | 1.4M |
| Time complexity (hour) | 0.19 | 0.24 | 2.0 | 12.3 | 4.6 |

The elements in hidden representations are often referred to as "channels" in CNNs and "neurons" in FNNs

VI. CONCLUSION

In this work, we proposed a GNN-based architecture to jointly optimize spatial-frequency user scheduling, hybrid precoding, and analog combining in MU-MIMO OFDM systems. The architecture consists of two cascaded modules dedicated to learning the discrete scheduling policy and the hybrid precoding policy, enabling joint training of the two modules to enhance overall learning performance. We discovered a sameparameter same-decision (SPSD) property for the wireless policies defined on sets. We found that a GNN cannot well learn the non-SPSD scheduling policy for users with similar channels, and proposed a sequence of GNNs for the scheduler module to improve the performance in high-density user scenarios. We also found that the precoding policy is non-SPSD on the user set, hindering the generalizability of GNNs to the number of users. We then proposed a novel attention mechanism for the precoding module to better aggregate information from different multi-antenna users, which can be generalized to all sizes.

Simulation results showcased several advantages of the proposed architecture in practical systems. The architecture can achieve SE comparable to numerical algorithms but at remarkably shorter computing latency. The architecture can be well generalized to the numbers of users, RBs, and antennas at both the BS and users, avoiding the retraining for different system scales. The architecture requires much lower training complexity than other DNNs to achieve the same performance, facilitating fast adaptation to dynamic channel environments.

APPENDIX A

PROOF OF EXAMPLE 2

The power control problem can be expressed as P_2 : $\max_{p_1,p_2}\log_2(1+\frac{h_{11}p_1}{h_{12}p_2+\sigma^2})+\log_2(1+\frac{h_{22}p_2}{h_{21}p_1+\sigma^2})$, s.t. $0 \le p_1,p_2 \le P_{max}$, where $h_{11},\ h_{22},\ h_{12}$, and h_{21} are channel gains and P_{max} is the maximal transmit power of each transmitter. The optimal solution of problem P_2 is one of $(p_1,p_2)=(P_{max},0),\ (0,P_{max}),$ and (P_{max},P_{max}) [36], which can be obtained by comparing the SE achieved by the three combinations. Further considering the same-parameter assumption, which implies a symmetric channel characterized by $h_{11}=h_{22}=h_T$ and $h_{12}=h_{21}=h_I$, the optimal solution depends on a threshold $s_h=2/(\sqrt{h_T^2+4h_I^2}-h_T)$. Specifically, the optimal solution is $(p_1,p_2)=(P_{max},P_{max})$ when $s_h>P_{max}/\sigma^2$, the optimal solutions are $(P_{max},0)$ and $(0,P_{max})$ when $s_h< P_{max}/\sigma^2$, and are all the three combinations when $s_h=P_{max}/\sigma^2$.

REFERENCES

- S. Liu and C. Yang, "Learning user scheduling and hybrid precoding with sequential graph neural network," *IEEE WCNC*, 2024.
- [2] R. W. Heath, N. González-Prelcic, S. Rangan, W. Roh, and A. M. Sayeed, "An overview of signal processing techniques for millimeter wave MIMO systems," *IEEE J. Sel. Top. Signal Process.*, vol. 10, no. 3, pp. 436–453, Apr. 2016.
- [3] X. Yu, J.-C. Shen, J. Zhang, and K. B. Letaief, "Alternating minimization algorithms for hybrid precoding in millimeter wave MIMO systems," *IEEE J. Sel. Top. Signal Process.*, vol. 10, no. 3, pp. 485–500, Apr. 2016.
- [4] Q. An, S. Segarra, C. Dick, A. Sabharwal, and R. Doost-Mohammady, "A deep reinforcement learning-based resource scheduler for massive MIMO networks," *IEEE Trans. Mach. Learn. Commun. Netw.*, vol. 1, pp. 242–257, 2023.
- [5] J. P. González-Coma, W. Utschick, and L. Castedo, "Hybrid LISA for wideband multiuser millimeter-wave communication systems under beam squint," *IEEE Trans. Wireless Commun.*, vol. 18, no. 2, pp. 1277– 1288, Feb. 2019.
- [6] T. E. Bogale, L. B. Le, A. Haghighat, and L. Vandendorpe, "On the number of RF chains and phase shifters, and scheduling design with hybrid analog-digital beamforming," *IEEE Trans. Wireless Commun.*, vol. 15, no. 5, pp. 3311–3326, May 2016.
- [7] L. Kong, S. Han, and C. Yang, "Wideband hybrid precoder for massive MIMO systems," *IEEE GlobalSIP*, 2015.
- [8] M. Mohammadkarimi, M. Darabi, and B. Maham, "User scheduling in massive MIMO: A joint deep learning and genetic algorithm approach," *IEEE VTC-Spring*, 2022.
- [9] B. Song, Z. Zhou, C. Li, D. Guo, X. Fu, and M. Hong, "Transformer based approach for wireless resource allocation problems involving mixed discrete and continuous variables," *IEEE SPAWC*, 2023.
- [10] I. M. Braga, E. d. O. Cavalcante, G. Fodor, Y. C. B. Silva, C. F. M. e Silva, and W. C. Freitas, "User scheduling based on multi-agent deep Q-learning for robust beamforming in multicell MISO systems," *IEEE Commun. Lett.*, vol. 24, no. 12, pp. 2809–2813, Dec. 2020.
- [11] W. V. F. Mauricio, T. F. Maciel, A. Klein, and F. R. M. Lima, "Scheduling for massive MIMO with hybrid precoding using contextual multi-armed bandits," *IEEE Trans. Veh. Technol.*, vol. 71, no. 7, pp. 7397–7413, Jul. 2022.

- [12] A. Vaswani, N. Shazeer, N. Parmar, J. Uszkoreit, L. Jones, A. N. Gomez, Ł. Kaiser, and I. Polosukhin, "Attention is all you need," NIPS, 2017.
- [13] Y. Yan, B. Zhang, C. Li, J. Bai, and Z. Yao, "A novel model-assisted decentralized multi-agent reinforcement learning for joint optimization of hybrid beamforming in massive MIMO mmWave systems," *IEEE Trans. Veh. Technol.*, vol. 72, no. 11, pp. 14743–14755, Nov. 2023.
- [14] Z. Zhang, T. Jiang, and W. Yu, "Learning based user scheduling in reconfigurable intelligent surface assisted multiuser downlink," *IEEE J. Sel. Top. Signal Process.*, vol. 16, no. 5, pp. 1026–1039, Aug. 2022.
- [15] R. Huang and V. W. S. Wong, "Joint user scheduling, phase shift control, and beamforming optimization in intelligent reflecting surface-aided systems," *IEEE Trans. Wireless Commun.*, vol. 21, no. 9, pp. 7521– 7535, Sep. 2022.
- [16] S. He, J. Yuan, Z. An, W. Huang, Y. Huang, and Y. Zhang, "Joint user scheduling and beamforming design for multiuser MISO downlink systems," *IEEE Trans. Wireless Commun.*, vol. 22, no. 5, pp. 2975–2988, May 2023.
- [17] M. Lee, G. Yu, H. Dai, and G. Y. Li, "Graph neural networks meet wireless communications: Motivation, applications, and future directions," *IEEE Wireless Commun.*, vol. 29, no. 5, pp. 12–19, Oct. 2022.
- [18] J. Guo and C. Yang, "A model-based GNN for learning precoding," *IEEE Trans. Wireless Commun.*, vol. 23, no. 7, pp. 6983–6999, Jul. 2024.
- [19] S. Liu, J. Guo, and C. Yang, "Multidimensional graph neural networks for wireless communications," *IEEE Trans. Wireless Commun.*, vol. 23, no. 4, pp. 3057–3073, Apr. 2024.
- [20] B. Zhao, J. Guo, and C. Yang, "Understanding the performance of learning precoding policies with graph and convolutional neural networks," *IEEE Trans. Commun.*, vol. 72, no. 9, pp. 5657–5673, Sep. 2024.
- [21] H. Jiang, Y. Lu, X. Li, B. Wang, Y. Zhou, and L. Dai, "Attention-based hybrid precoding for mmWave MIMO systems," *IEEE ITW*, 2021.
- [22] Y. Li, Y. Lu, B. Ai, O. A. Dobre, Z. Ding, and D. Niyato, "GNN-based beamforming for sum-rate maximization in MU-MISO networks," *IEEE Trans. Wireless Commun.*, vol. 23, no. 8, pp. 9251–9264, Aug. 2024.
- [23] Y. Li, Y. Lu, R. Zhang, B. Ai, and Z. Zhong, "Deep learning for energy efficient beamforming in MU-MISO networks: A GAT-based approach," *IEEE Wireless Commun. Lett.*, vol. 12, no. 7, pp. 1264–1268, Jul. 2023.
- [24] P. Veličković, G. Cucurull, A. Casanova, A. Romero, P. Lio, and Y. Bengio, "Graph attention networks," ICML, 2018.
- [25] Y. Li and Y.-F. Liu, "HPE transformer: Learning to optimize multi-group multicast beamforming under nonconvex QoS constraints," *IEEE Trans. Commun.*, vol. 72, no. 9, pp. 5581–5594, Sep. 2024.
- [26] H. Yuan, J. An, N. Yang, K. Yang, and T. Q. Duong, "Low complexity hybrid precoding for multiuser millimeter wave systems over frequency selective channels," *IEEE Trans. Veh. Technol.*, vol. 68, no. 1, pp. 983– 987, Jan. 2019.
- [27] C. Sun and C. Yang, "Learning to optimize with unsupervised learning: Training deep neural networks for URLLC," IEEE PIMRC, 2019.
- [28] T. Yoo and A. Goldsmith, "On the optimality of multiantenna broad-cast scheduling using zero-forcing beamforming," *IEEE J. Sel. Areas Commun.*, vol. 24, no. 3, pp. 528–541, Mar. 2006.
- [29] S. M. Xie and S. Ermon, "Reparameterizable subset sampling via continuous relaxations," *IJCAI*, 2019.
- [30] E. Conte, S. Tomasin, and N. Benvenuto, "A simplified greedy algorithm for joint scheduling and beamforming in multiuser MIMO OFDM," *IEEE Commun. Lett.*, vol. 14, no. 5, pp. 381–383, May 2010.
- [31] X. Zhao, T. Lin, Y. Zhu, and J. Zhang, "Partially-connected hybrid beamforming for spectral efficiency maximization via a weighted MMSE equivalence," *IEEE Trans. Wireless Commun.*, vol. 20, no. 12, pp. 8218– 8232, Dec. 2021.
- [32] Y. Liu and J. Wang, "Low-complexity OFDM-based hybrid precoding for multiuser massive MIMO systems," *IEEE Wireless Commun. Lett.*, vol. 9, no. 3, pp. 263–266, Mar. 2020.
- [33] O. E. Ayach, S. Rajagopal, S. Abu-Surra, Z. Pi, and R. W. Heath, "Spatially sparse precoding in millimeter wave MIMO systems," *IEEE Trans. Wireless Commun.*, vol. 13, no. 3, pp. 1499–1513, Mar. 2014.
- [34] 3GPP, "Study on channel model for frequencies from 0.5 to 100 GHz," TR 38.901, Version 17.0.0, Mar. 2022.
- [35] A. M. Elbir, K. V. Mishra, M. R. B. Shankar, and B. Ottersten, "A family of deep learning architectures for channel estimation and hybrid beamforming in multi-carrier mm-wave massive MIMO," *IEEE Trans. Cogn. Commun. Netw.*, vol. 8, no. 2, pp. 642–656, Jun. 2022.
- [36] Z.-Q. Luo and S. Zhang, "Dynamic spectrum management: Complexity and duality," *IEEE J. Sel. Top. Signal Process.*, vol. 2, no. 1, pp. 57–73, Feb. 2008.